



Comparing the Porosities of Upper Red Sandstone and Asmari Limestone using Petrographic Image Analysis and Saturation-Buoyancy Methods

Saeed Nejadi, Mashallah Khomehchiyan *, Mohammad Reza Nikudel, Ahmad Zalooli 

Department of Geology, Faculty of Basic Science, Tarbiat Modares University, Tehran 14155-111, Iran

Received: 29 March 2023, Revised: 19 August 2023, Accepted: 02 September 2023

© University of Tehran

Abstract

This study compares rock porosities measured using petrographic image analysis (PIA) and saturation-buoyancy (SB) methods. To this end, the fresh block samples from sandstone and limestone were collected from Upper Red and Asmari Formations, respectively. Next, cylindrical core specimens from those were prepared using a coring machine. Afterward, the porosity values of sandstone and limestone samples were measured using PIA and SB methods. In the next step, the physical and mechanical properties of samples, including water absorption (W), P wave velocity (PWV), uniaxial compressive strength (UCS), Young's modulus (E), point load strength index (PLSI), and Brazilian tensile strength (BTS), were determined. Results showed that PIA underestimates the porosity in both rocks. These conservative results can be attributed to the incomplete filling of micropores with blue-dyed epoxy resin in sandstone cement and limestone matrix or petrographic microscope limitation to differentiate micropores in cement and matrix. Furthermore, results demonstrated that SB in upper red sandstone has a good correlation with W, E, and BTS and a moderate correlation with PWV, UCS, and PLSI. Besides, porosity of limestone samples showed strong relation with W, PWV, and BTS, while UCS and E data versus porosity showed a scattering pattern. Finally, a strong relation was established between PIA porosity and UCS, E, and PLSI, a poor correlation was established in the cases of W, PWV, and BTS. Overall, PIA is a strong method for investigating the interior pore system of rocks, especially isolated pore spaces, although it underestimates rocks porosity compared to the SB method.

Keywords: Petrographic Image Analysis; Porosity; Upper Red Sandstone; Asmari Limestone; Physico-Mechanical Properties.

Introduction

Sedimentary rocks as the most abundant type of rock forming 70% of the earth's surface (Tucker 2009). Asmari Formation, as the most important oil reservoir in the Zagros zone (south west of Iran), has been widely studied (Wennberg et al., 2006; Ahmadhadi et al., 2008; Najibi et al., 2015; Moradi et al., 2017). Sandstone from Upper Red Formation has been used as heritage stone mainly in rural areas for building farm walls (Khanlari and Abdilor 2015; Khanlari et al., 2015; Ghobadi and Babazadeh 2015a,b, 2016).

Porosity, i.e., the ratio of void volume to the total volume of a rock, is an important property of sandstone and carbonate rocks. These rocks exhibit two major kinds of porosity, including primary and secondary porosity. Primary porosity is generated during deposition and classified as intergranular or intragranular porosity. Secondary porosity is generated after deposition by

* Corresponding author e-mail: khamechm@modares.ac.ir

different processes such as dissolution of the primary detrital grains, weathering processes, or in situ stresses (Pettijohn 1975; Paxton et al., 2002; Scholle and Ulmer-Scholle 2003; Farrell et al., 2014; Zalooli et al., 2018a, 2020, Shaeri et al., 2022). There are several methods for measuring the porosity in different rocks, including saturation and buoyancy, mercury intrusion porosimetry, gas adsorption, X-ray microtomography, nuclear magnetic resonance (NMR), petrographic image analysis, point counting techniques, and scanning electron microscopy (SEM). The saturation and buoyancy is a common non-destructive method that estimates both total and effective porosities without providing any image of pore shape and structure. This method is suitable for rocks that do not deteriorate when submerged in water (ISRM 2007). Mercury porosimetry test is a destructive method to measure effective porosity and provide pore size distribution of rocks (Freire-Lista et al., 2016). This technique is appropriate for measuring the porosity of intact or hard rocks (James 1995; Cerepi et al., 2001). In the case of gas adsorption, the mean pore radius is calculated if the shape of the pores is assumed rounded. However, this approach could not measure the isolated pores (Higgins 2006). Despite the resolution limitations of X-ray microtomography, it is a non-destructive technique that provides information about the distribution of pore sizes and measures the total porosity (Alves et al., 2014). Another effective method for this purpose is Petrographic Image Analysis, which measures total porosity (Haines et al., 2015). Since many researchers all over the world use the PIA in their investigations (Anselmetti et al., 1998; Cerepi et al., 2001; Assefa et al., 2003; Perring et al., 2004; Obara 2007; Lima Neto et al., 2014; Berrezueta et al., 2015). Grove and Jerram (2011) reported that estimated porosities by PIA generally confirm the results of the point counting method despite the differences between them. Ghiasi-Freez et al. (2012) used PIA to classify pore spaces using an intelligent discriminant classifier. Berrezueta et al. (2015) stated that PIA is an effective, accurate, and easy way to evaluate porosity and a statistically powerful method compared to the point counting method. Haines et al., (2015) verified that the image analysis method is a robust way for porosity assessment. Furthermore, pore system characteristics such as permeability of rocks and sediments can be evaluated and easily measured using the PIA procedure (Ruzyla 1986; James 1995; Solymar and Fabricius 1999 Nabawy 2014; Peng et al., 2016; Rabbani et al., 2017).

Porosity is an important parameter influencing physical and mechanical properties (Tuğrul and Zarif 1999; Tuğrul 2004; Jeng et al., 2004; Kahraman et al., 2005; Pappalardo et al., 2017; Jamshidi et al., 2018, Ghasemi et al., 2021; Jamshidi 2022), such as susceptibility to weathering (Benavente et al., 2004; Di Benedetto et al., 2015; Zalooli et al. 2017; Freire-lista et al., 2015, 2022; Jamshidi et al., 2013; 2015; 2016, 2017) and hydraulic conductivity of rocks (Boving and Grathwohl 2001).

Previous studies have mainly focused on measuring the porosity values, especially pore space properties, using PIA and the effect of pore properties on other parameters in various rock types. However, rare studies are available concerning the differences between porosities evaluated by PIA and those measured using the saturation-buoyancy method.

Regarding the importance of the Asmari Limestone (AL) and Upper Red Sandstone (URS) in Iran, the present study compares porosities obtained by PIA and saturation-buoyancy methods in these formations. Then, the influence of porosity on the physical and mechanical properties of URS and AL is investigated by establishing a correlation between these variables.

Sample database

Fresh samples with no visible fractures were collected from Avaj region (URS outcrops) and Asmari village (AL outcrops), located in the southwest of Qazvin Province and northeast of Khuzestan Province, respectively (Fig. 1). Four blocks with the dimension of approximately 40 cm × 40 cm × 40 cm were selected from each formation.

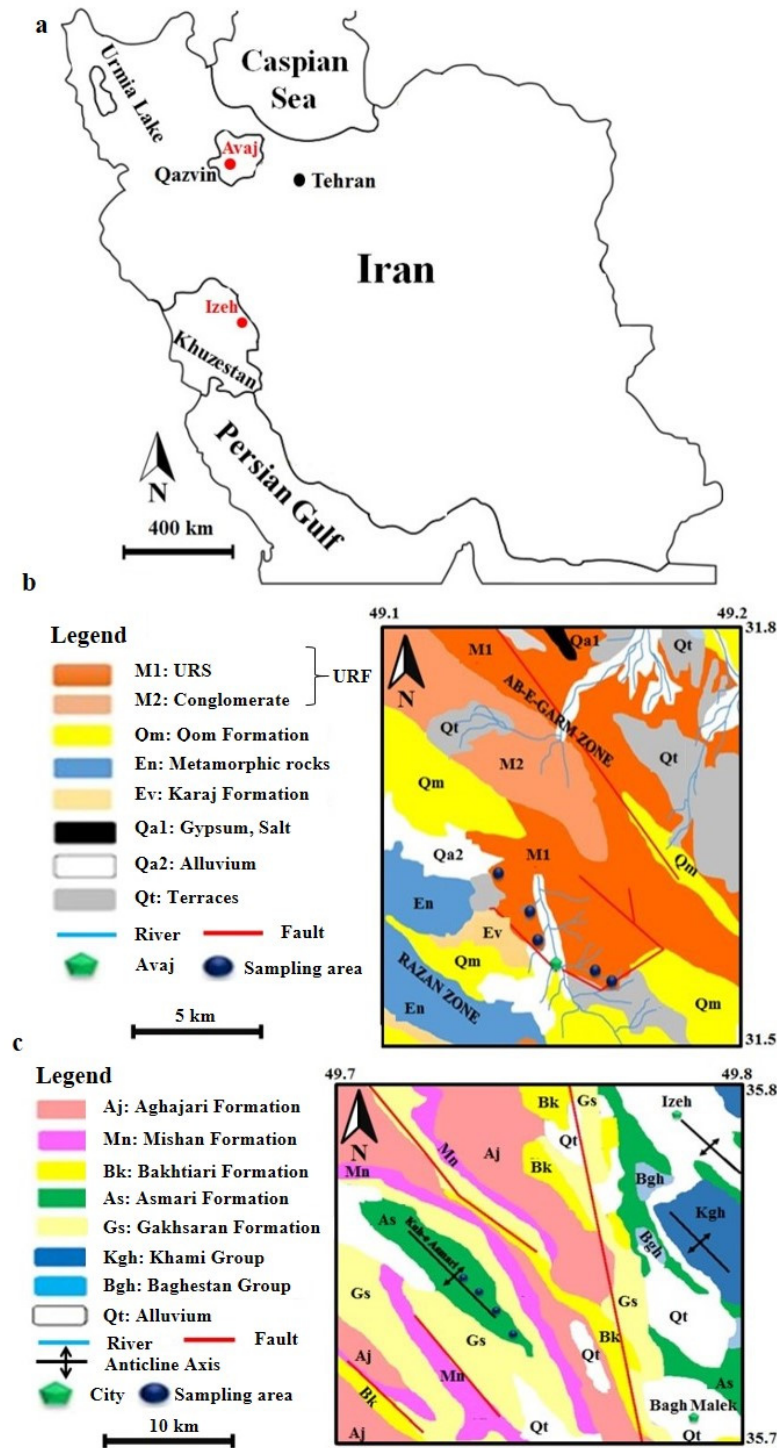


Figure 1. Geographical map of Iran (a) and sampling areas in Avaj (b) and Asmari regions (c)

Geological setting

The Asmari Formation is the most important petroleum reservoir formation in the Zagros zone, extending from the northwest to the southeast of Iran. In the Asmari region, limestones are mainly creamy to brown, with a thickness reaching 314 m. With an age of the Miocene epoch, this

formation is well-known for its tectonically-induced joints. This formation was the first reservoir in the middle east used for petroleum extraction (Motiei 1993; Dehghanian et al., 2012).

The upper Red Formation, outcropped in some parts of the central Iran Zone, belongs to the Miocene epoch and is comprised of mainly sandstone, marl, conglomerate, and evaporates. This formation covers the vast area within the central Iran basins, such as the central desert of Iran (Khosrow Tehrani 1989; Lasemy 1990). In the Avaj area, Upper Red Formation consists of red sandstone and shale successions. Weathering and erosion have produced low-altitude hills in areas where shale is dominant. Meanwhile, high cliffs are characteristic of terrain comprising red sandstones. The approximate thickness of red sandstone layers in the sampling area reaches 0.75 m-1 m.

Material and methodology

Sample preparation

Cylindrical samples with a diameter of 54 mm and length-to-diameter ratios of 2.5, 1, and 0.5 were prepared. Sample ends were cut and polished parallel to each other and perpendicular to the sides using a low-speed diamond blade saw (120 rpm). These samples were used to determine the physical and mechanical characteristics of the rocks.

Thin-section studies

For each sample, specimens were cut in three directions to prepare thin sections. To distinguish the pore from solid parts, samples were impregnated with epoxy resin containing 1% blue dye. Petrographic analysis was performed under a polarized microscope in accordance with a previous study (Ghiasi-Freez et al., 2012; Rabbani et al., 2017). Both Upper Red Sandstone (URS) and Asmari Limestone (AL) block samples were named using the percentage of main components. The URS samples were classified according to the Folk (1974) diagram. Also, Dunham (1962) and Folk (1962) classifications were applied to name the AL samples.

Image processing

Fig. 2 presents the steps of image processing conducted in this work: 1) digital image acquisition, 2) image pre-processing, 3) setting image threshold, and 4) statistical analysis.

Image acquisition

Thin sections were examined under a Bell polarized microscope equipped with a 3-MP resolution digital camera. Above 90 images under a polarized microscope (PM) at a magnification of 40 \times were captured from each orientation (x, y, and z). Finally, PM micrograph mosaics were made from each thin section (Fig. 3a and Fig. 4a).

Image pre-processing

The magnification of the image has a large impact on PIA porosity value (Andriani and Walsh 2002; Haines et al., 2015). In other words, The more magnification, the higher the porosity value (Haines et al., 2015). The first step in image pre-processing procedure is to crop the image. This means that irrelevant parts of the image must be removed so that the focus is on the area of interest (Přikryl 2006). Those parts located on the edges of the image with incompletely filled voids or with voids containing pockets of air were removed.

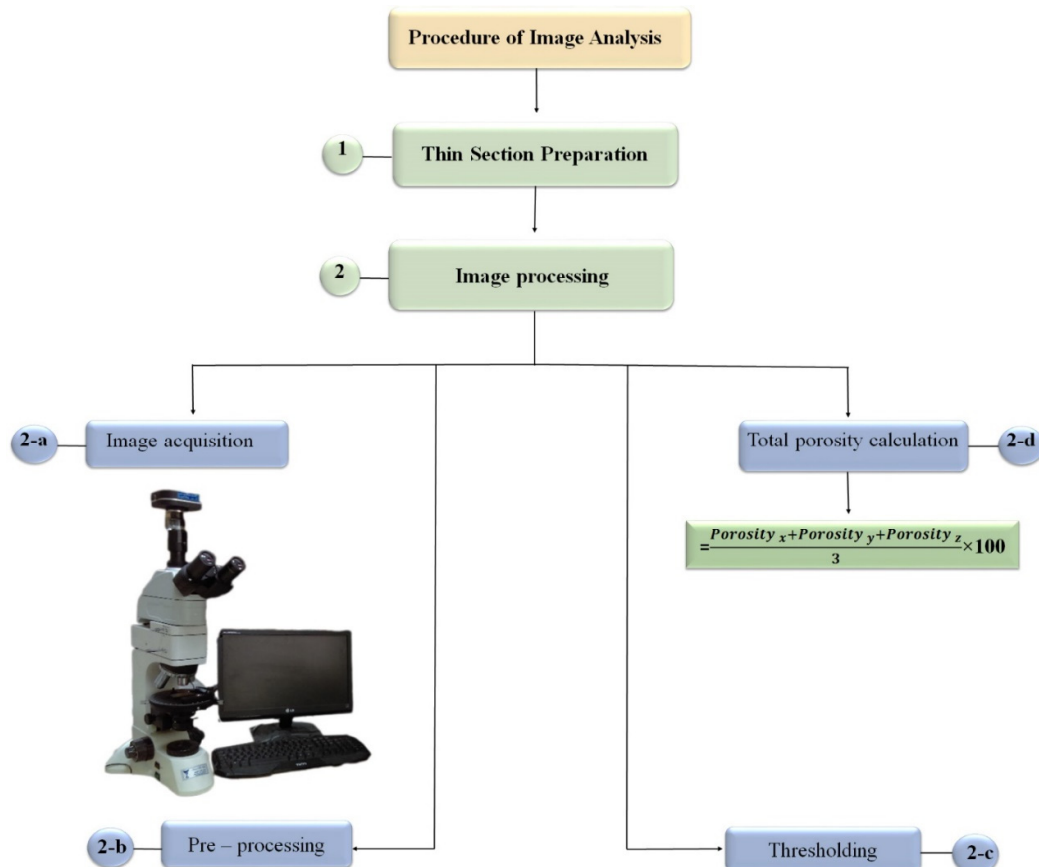


Figure 2. The flowchart of the image analysis process followed in this study

Thresholding

The porosity can be calculated through image analysis by converting the prepared images to binary formats to show pore spaces versus mineral phases. After pore spaces were modified as red-colored spaces using ImageJ software (Fig. 3b and Fig. 4b). The image must be separated into red, green, and blue components (Andriani and Walsh 2002), and then the image should be thresholded to a two-bit image where the voids are black and matrix is white. All pixels in the image whose values lie under the threshold value are converted to black (pore spaces) and all pixels with values above the threshold are converted to white (matrix) (Fig. 3c and Fig. 4c). Finally, the porosity percentage was calculated from the ratio of black areas to total area of pixels as follows (Eq. 1):

$$\text{porosity } (n) = \frac{\text{Total area of black pixels}}{\text{Total area of pixels}} \times 100 \quad (1)$$

Statistical analysis

The average porosity of each rock is the result of the average porosity in three directions of x, y, and z (Eq. 2):

$$\text{Porosity } (n) = \frac{\text{Porosity}_x + \text{Porosity}_y + \text{Porosity}_z}{3} \times 100 \quad (2)$$

Physical properties

Cylindrical specimens with a diameter of 54 mm and a length-to-diameter ratio of 2.5 were

used to determine the total porosity and water absorption. Overall, 30 core specimens from URS and 15 from AL were prepared. These properties were measured by saturation-buoyancy technique according to ISRM (2007) using saturated-submerged mass (M_{sub}), saturated-surface-dry mass (M_{sat}), and dry mass (M_{dry}) calculation.

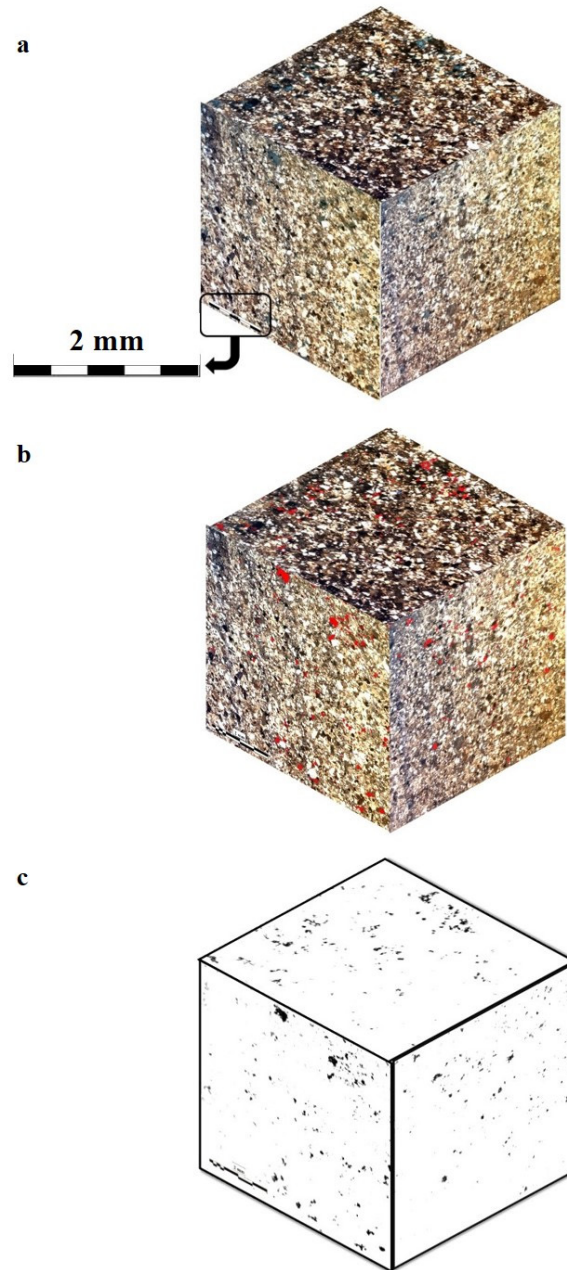


Figure 3. a) 3D view of sample SS-1 (belonging to URS) interior in pre-processing step; the pore spaces are filled by blue-dyed epoxy resin, and the rest contains mineral phases; b) Converting the blue-colored pore areas to red to assess pore space pixels appropriately; c) Thresholded 3D view of sample SS-1 interior ready for porosity calculation; here, the porosity is measured as the ratio of the total area of the black pixels divided by the total area of the photo

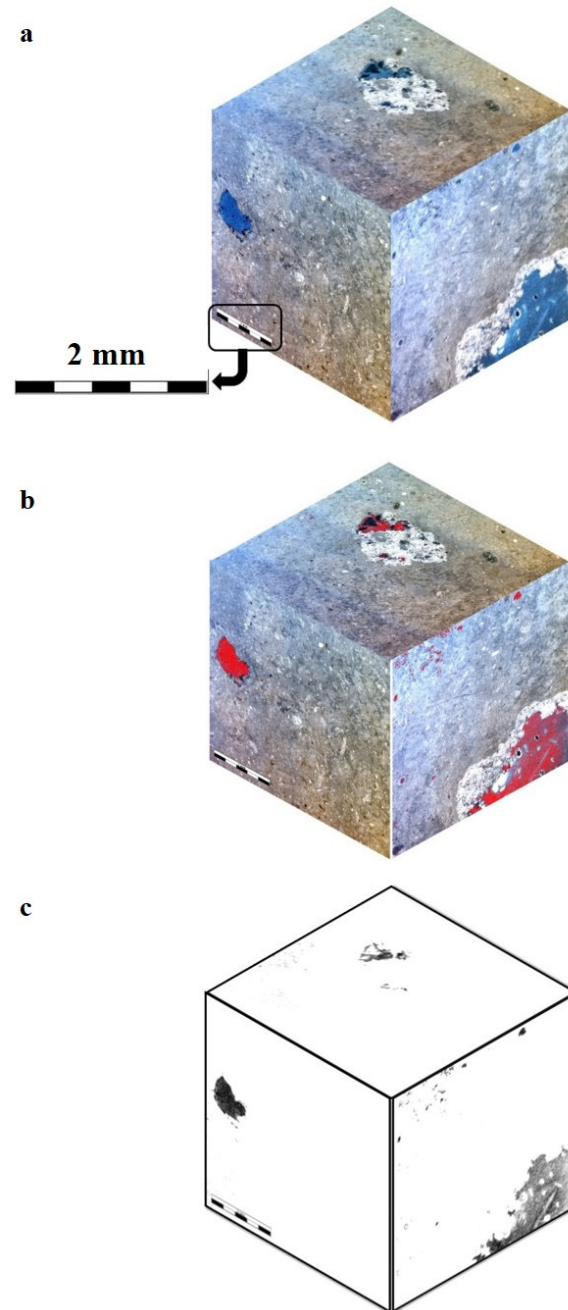


Figure 4. a) 3D view of sample LS-3 (belonging to AL) interior in the pre-processing step; the pore spaces are filled by blue-dyed epoxy resin and the rest includes the mineral phases; b) Converting the blue-colored pore areas to the red to assess pore spaces pixels appropriately; c) Thresholded 3D view of sample LS-3 interior, ready to porosity calculation

To measure M_{sub} , specimens were placed in a basket in an immersion bath. Then, M_{sat} specimens were saturated with water under the vacuum pressure of 800 Pa for 24 h. Finally, specimens were dried at 105°C for 24 h to measure M_{dry} . Eq. (3) was used to calculate the total volume (V) of a specimen:

$$V = \left(\frac{M_{\text{sat}} - M_{\text{sub}}}{\rho_w} \right) \quad (3)$$

where the ρ_w is water density.

Total porosity (TP) was calculated by Eq. (4):

$$TP = \left(1 - \left(\frac{\rho_{dry}}{\rho_s} \right) \right) \times 100 \quad (4)$$

where ρ_{dry} and ρ_s are dry density and solid density calculated by Eqs. (5) and (6), respectively:

$$\rho_{dry} = \left(\frac{M_{dry}}{V} \right) \quad (5)$$

$$\rho_s = G_s \times \rho_w \quad (6)$$

where G_s is the specific gravity measured according to ISRM (2007).

Water absorption (W_a) was determined according to the formula proposed by ISRM (2007) (Eq.7):

$$W_a = \left(\frac{M_{sat} - M_{dry}}{M_{dry}} \right) \times 100 \quad (7)$$

P-wave velocity

P-wave velocity was measured both in dry and saturated conditions in each specimen by ultrasonic compressional wave according to the ISRM (2007). To this end, 30 URS and 15 AL core specimens were used. All the specimens were 54 mm in diameter and had a length-to-diameter ratio of 2.5. An ultrasonic gel was rubbed at the two ends of cylindrical specimens to make a smooth surface.

Mechanical properties

In this study, 3 cylindrical specimens from each sandstone and limestone block (24 core specimens in total) were tested under a UCS tester following the ISRM (2007) recommendations. UCS tests were carried out on dry specimens with a loading rate of 0.5 MPa/s. In the layered specimens, the loading direction was perpendicular to the anisotropic plane. The axial displacement of specimens subjected to uniaxial loading was recorded using an axial gauge. From the stress-strain curve, E was calculated for each specimen as the tangent of the mentioned curve.

PLSI was determined by preparing 3 specimens from each block sample (a total of 24 core specimens). Since sandstone core specimens had the weakness planes, the direction of the point load was kept perpendicular to the planes. In the next step, 3 dry specimens with a diameter from each block specimen (24 planar specimens in total) were used to measure Brazilian tensile strength (BTS).

Regression analysis

The mean values of PLSI and BTS derived from each block sample were used to establish a logical relation between obtained results and porosity values.

Results and Discussions

Petrographic studies

The results of petrographic studies are given in Table 1 and Table 2 and Figs. 5-7. The location of URS samples on the Folk diagram is illustrated in Fig. 6. In this study, to avoid misunderstanding and confusion, we abbreviated URS and AL samples to SS (sandstone) and LS (limestone), respectively.

Table 1. Components of URS samples (SS-1 to SS-4) obtained from the thin section study and their names according to the Folk (1974) classification

Sample	Components (%)							Name
	Quartz	Feldspar	Lithic	Opaque	Mica	Clay Cement	unidentified particles	
SS-1	33.85	9.47	23.69	12.86	8.46	5.07	3.04	Feldspathic litharenite
SS-2	23.39	10.23	30.7	4.38	7.3	11.69	11.69	Litharenite
SS-3	26.65	8.88	35.54	5.92	5.92	16.29	0	Litharenite
SS-4	16.27	13.01	38.08	4.88	4.88	14.64	6.5	Feldspathic litharenite

Table 2. Components of AL samples (LS-1 to LS-4), from the thin-section study of and their names according to the Dunham (1962) and Folk (1962) classifications

Sample	Components (%)					Dunham Classification	Folk classification
	Micrite	Quartz	Fossil content	Fe oxide	Other unidentified components		
LS-1	90	0	5	0	5	Mudstone	Bioclasts micrite
LS-2	75.6	0	14.6	4.87	4.87	Wackestone	Biomicrite
LS-3	70.2	3.42	5.13	5.82	15.41	Wackestone	Biomicrite
LS-4	93.26	0	4.8	0	1.92	Mudstone	Bioclasts micrite

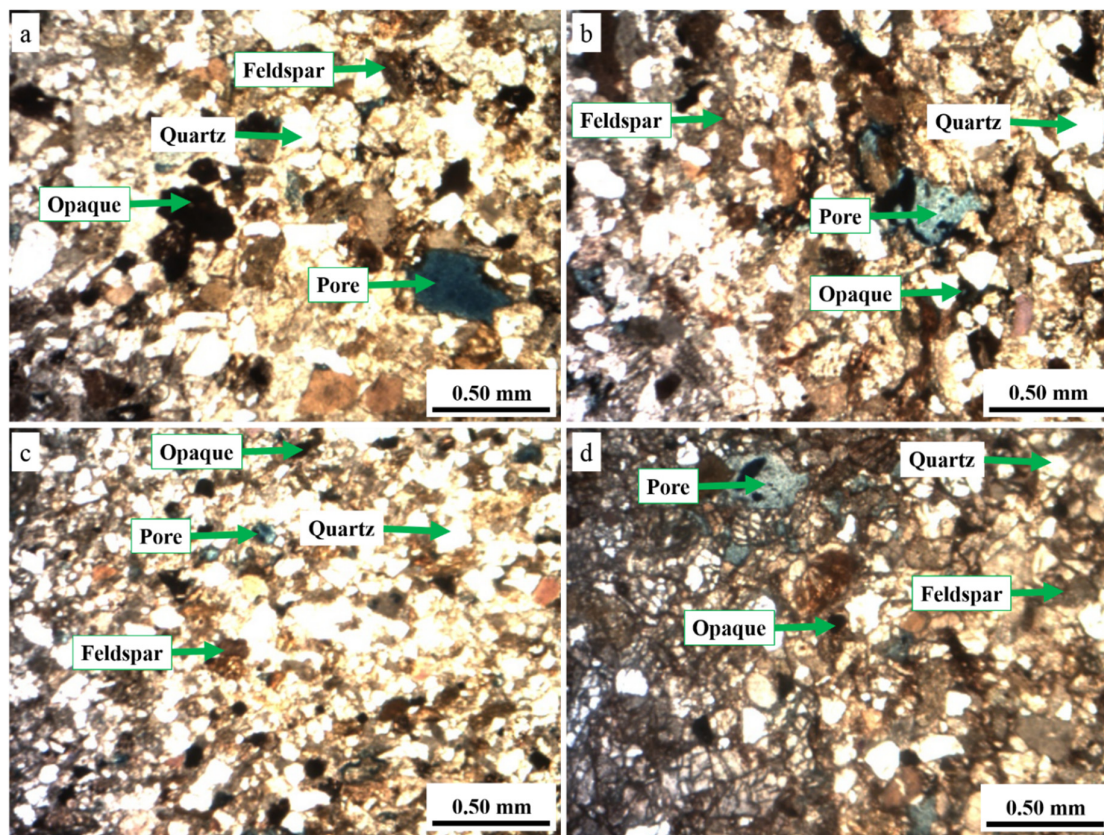


Figure 5. Photomicrographs of sandstones under the polarized microscope: a) SS-1, b) SS-2, c) SS-3, and d) SS-4

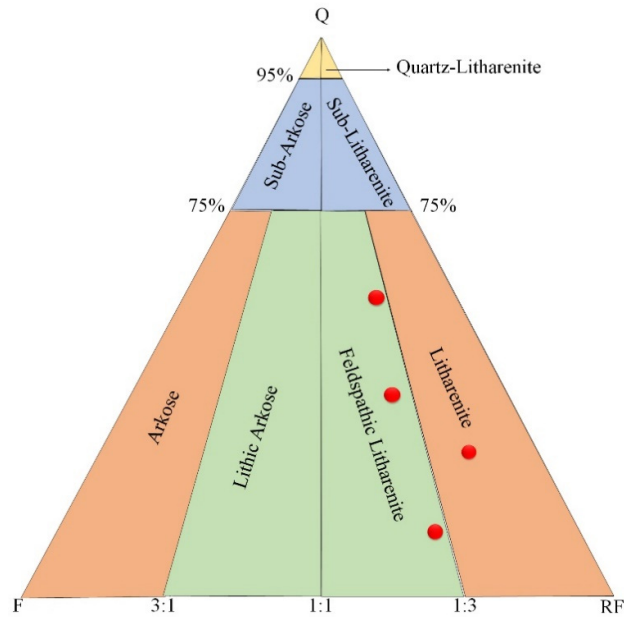


Figure 6. Classification of URS samples (red points) based on Folk's (1974) classification system

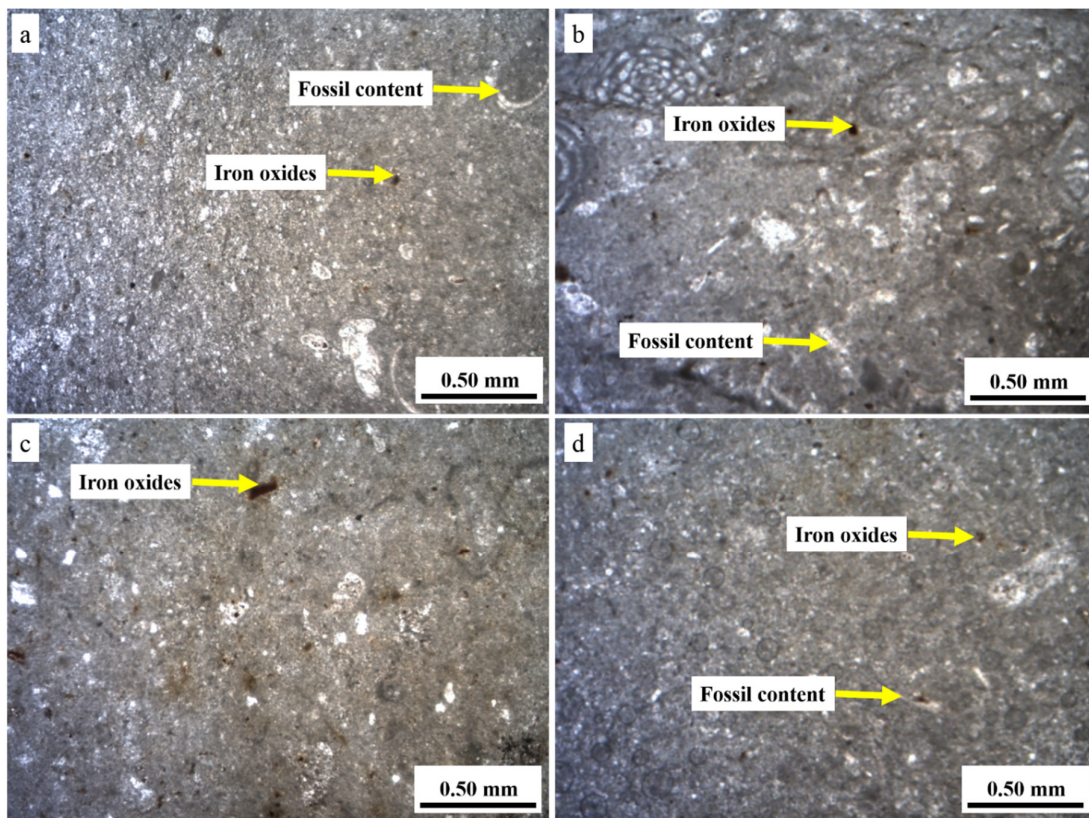


Figure 7. Photomicrographs of limestones under the polarized microscope: a) LS-1, b) LS-2, c) LS-3, and d) LS-4

Physical and mechanical properties

Table 3 shows the results of the physical and mechanical properties of URS and AL samples. Water absorption in URS samples range from 0.93% to 3.17% with an average value of 1.85%,

while it ranges from 0.06% to 1.87% with an average value of 0.93% in AL samples. Effective porosity obtained from SB method in URS samples changes from 2.28% to 7.41%, while it ranges from 0.17% to 4.7% in AL samples. The mean dry PWV was found to be 3862 m/s and 3908 m/s in URS and AL samples. PWV increased in both sample when they were saturated. Saturation causes the PWV to rise in all samples as the P wave can rapidly pass through the saturated media. The mean saturated PWV of URS and AL samples was 4252 m/s and 4900 m/s, respectively. Both samples exhibited relatively the identical value of UCS, PLSI and BTS. AL had higher E than URS sample.

Porosity measurement using PIA

Results of porosity calculation by using the PIA in URS and AL samples are listed in Table 4 and Fig. 8. Porosity obtained from PIA changes from 0.67% to 3.47% with an average value of 1.67 % for URS. In AL samples, PIA (blue bar) shows zero values in samples LS-1, LS-2, and LS-4. However, in sample LS-3, the porosity value from PIA is close to the value from SB (green bar), and it is more than 2% in both methods. Porosity underestimation in LS-1, LS-2, and LS-4 from PIA results is because of the failure of the PIA method to measure the micropore spaces from the matrix where blue-dyed epoxy resin cannot penetrate or pores can not be detected due to insufficient resolution of petrography microscope (Haines et al., 2015). In comparison, in the SB method, since the matrix can absorb water, SB can display more amount of porosity values, especially in samples LS-1, LS-2, and LS-4. These samples are micrite-dominated and can absorb a considerable amount of water in their structure. Moldic, vuggy, interparticle, and intraparticle are the main types of porosity shapes in limestones (Choquette and Pray, 1970; Lima Neto et al., 2014). In the AL samples, only LS-3 showed vuggy porosity, which was recognized by the PIA.

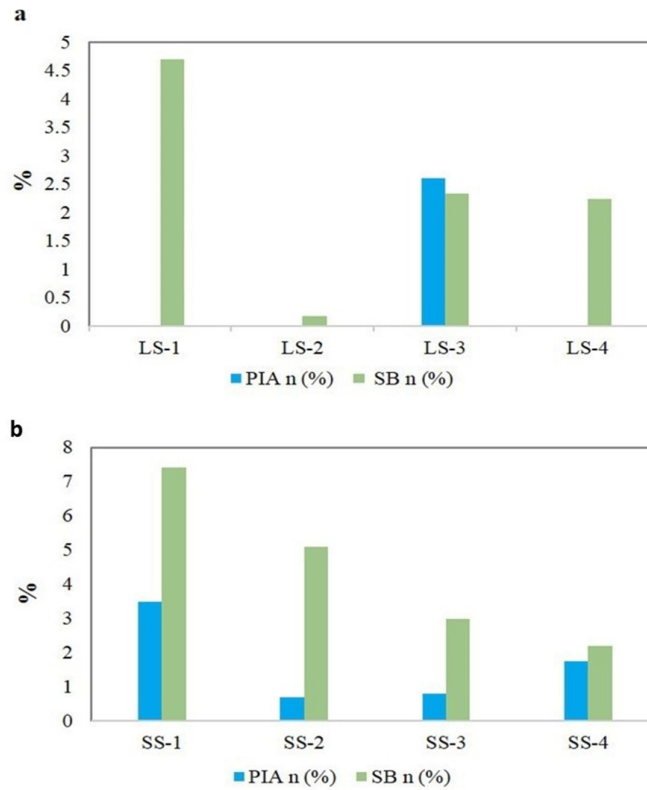
As shown in Fig 8b, in URS samples, porosities from SB (green bar) show a decreasing trend from samples of SS-1 (7.41%) to SS-4 (2.18%). On the contrary, the porosity calculated by PIA (blue bar) for the SS-1 sample has the highest value (3.47%).

Table 3. Mean values of physical and mechanical test results, including water absorption (W), saturation-buoyancy porosity (n), p-wave velocity (PWV) in dry and saturated conditions, uniaxial compressive strength (UCS), Young's modulus (E), point load strength index (PLSI), and Brazilian tensile strength (BTS) on URS and AL samples

Sample		Physical Tests				Mechanical Tests			
		W	n	Dry PWV	Saturated PWV	USC	E	PLSI	BTS
Type	Name	(%)	(%)	(m/s)	(m/s)	(MPa)	(GPa)	(MPa)	(MPa)
URS	SS-1	3.17	7.41	4270	4300	72.8	3.44	2.93	8.56
	SS-2	2.12	5.08	2790	3800	110.1	15.72	4.84	10.33
	SS-3	1.18	2.98	4120	4610	88.55	32.77	7.97	13.47
	SS-4	0.93	2.28	4270	4300	112	22.14	4.78	12.16
Average value		1.85	4.43	3862	4252	95.86	18.52	5.13	11.13
AL	LS-1	1.87	4.7	3430	4130	80.2	25.48	4.11	10.15
	LS-2	0.06	0.17	4480	5920	91.85	36.40	2.74	13.50
	LS-3	0.92	2.59	3880	4840	106.41	103.41	10.52	12.15
	LS-4	0.88	2.28	3840	4710	116.13	98.64	3.04	15.03
Average value		0.93	2.44	3908	4900	98.65	65.98	5.10	12.71

Table 4. Results of porosity calculated using the PIA in URS and Al samples

Sample	Sample Name	Petrographic Image Analysis Porosity (%)			
		X	Y	Z	Mean porosity
URS	SS-1	2.8	3.52	4.09	3.47
	SS-2	0.66	0.73	0.62	0.67
	SS-3	0.82	0.74	0.79	0.78
	SS-4	1.43	1.88	1.91	1.74
	Average value	1.43	1.72	1.85	1.67
AL	LS-1	0.00	0.00	0.00	0.00
	LS-2	0.00	0.00	0.00	0.00
	LS-3	1.59	0.76	5.47	2.6
	LS-4	0.00	0.00	0.00	0.00
	Average value	0.40	0.19	1.37	0.65

**Figure 8.** Porosity values obtained by PIA (blue bar) and SB (green bar) methods in AL (a) and URS (b) samples

Nevertheless, the porosity values of samples from SS-2 to SS-4 do not follow this trend for SB. In other words, PIA porosity values in samples SS-2 (0.67%) to SS-4 (1.74%) show a slightly increasing trend. Overall, porosity underestimation by PIA has the same reasons as the AL porosities. Unlike the study of Zalooli et al., (2018b), in which large pore spaces filled with water lost water rapidly during the SB method, and blue-dyed resin could easily enter them, in the present study, small-scale pores can keep more water during the test. As a result, the PIA method overestimates the porosity in the travertine samples (Zalooli et al., 2018b) and underestimates the porosity compared to the SB method in the studied sandstones.

The relation between SB porosity and other physical and mechanical properties

Both total and effective porosities are essential parts of rock mechanics and engineering

geology studies. Therefore, the relation between total porosity by SB in both URS and AL samples and other physical and mechanical properties was investigated. Porosity by itself can control other physical and mechanical features. In both sample, there is a positive linear relation between water absorption and SB porosity with high correlation coefficient ($R^2=0.99$). both in URS and AL samples. Previous studies have postulated that porosity is a key parameter controlling water absorption of rocks (Erdoğan and Özvan 2015). The explanation is that in the SB method, porosity is measured by water absorption in samples.

According to previous studies, porosity has a reverse relationship with PWV (Tuğrul and Zarif 1999; Sousa et al., 2005), and it can properly control PWV (Khanlari et al., 2015). In URS samples, a weak to fair relationship between porosity and PWVD in dry ($R^2= 0.47$) and saturated ($R^2= 0.52$) conditions was found (Figs. 9c, d). Meanwhile, a strong relationship is observed in AL samples ($R^2 \geq 0.95$) (Figs. 9e, f). This is due to the fact that PWV in the sandstones is mainly influenced by mineralogical content (Stueck et al., 2013), while porosity play an important role controlling PWV in carbonates (Török and Vásárhelyi 2010). Kassab and Weller (2015) showed a weak to fair inverse relationship between porosity and dry PWV with correlation coefficient of 0.46 in sandstones. In URS sample, the relationship was improved to be better than that in the dry case, where the correlation coefficient became 0.52. This is in accordance with Kassab and Weller (2015).

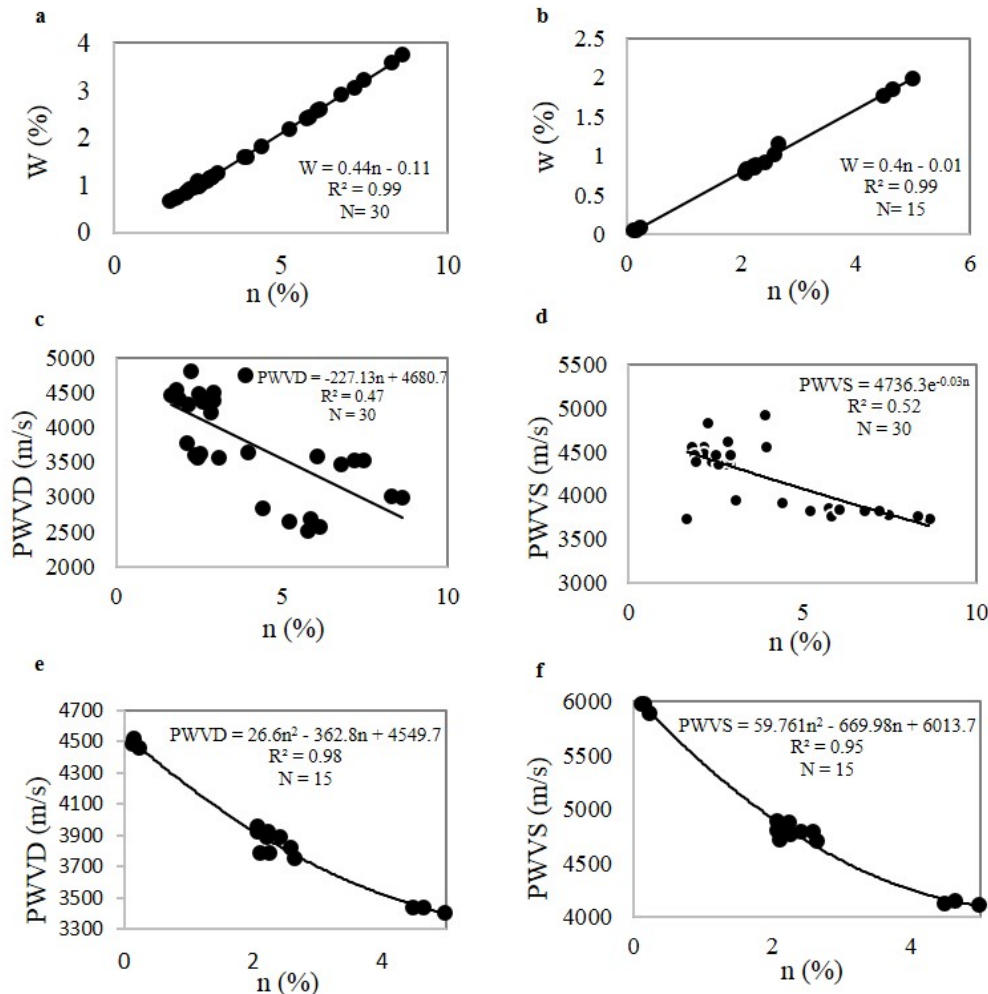


Figure 9. The relation between SB porosity and water absorption in a) URS samples and b) AL samples; The relation between SB porosity and c) PWVD in URS, d) PWVS in URS, e) PWVD in AL, and f) PWVS in AL samples

An increase in the porosity can lead to a reduction in UCS values (Bell and Lindsay 1999; Mishra and Basu 2013). Thus, porosity is a key feature in rock strength because the voids cause decreasing in materials integrity (Tuğrul and Zarif 1999). As shown in Fig. 10a, a weak inverse linear relation ($R^2=0.48$) was extracted between porosity with UCS in URS samples. This is due to the fact the UCS of sandstones is influenced by porosity, mineralogical content, cementation, packing density and grain contact (Chang et al., 2006). The empirical expressions for the UCS of sandstone and carbonates rocks are presented in Table 5, where the linear and exponential modes are applied in the regressions. As can be see, the correlation coefficient between porosity and UCS in previous studies changes from 0.28 to 0.88.

As given in Fig. 11a, contrary to URS, no distinguishable relation was determined between porosity and UCS in AL samples. However, Previous studies have shown a strong negative relationship between porosity and UCS in carbonates (Table 5). The samples with more porosities (LS-1) reveal less UCS compared to the samples with less porosities (LS-2). In comparison, in samples LS-3 and LS-4, large UCS values are obtained for moderate porosity values. This phenomenon clarifies that porosity is not the main factor controlling the UCS in AL. Like UCS, decreasing E could be due to the porosity increasing (Bell and Lindsay 1999). As shown in Fig. 10b, a reverse relation may be identified between porosity and E in URS samples. Pore spaces make the rock samples hollow and lower their E values. However, the behavior of AL samples is varied (Fig. 11b).

Table 5. Empirical expressions for UCS prediction based on porosity in sandstones and carbonate rocks

References	Expression	R ²	Samples
Qi et al. (2022)	$UCS = 110.5 \exp(-0.08 n)$	0.72	17 sandstone samples
Farrokhrouz and Asef (2017)	$UCS = -3.03 n + 107.1$	0.28	299 sandstone samples
Mishra and Basu (2013)	$UCS = -55.7 \ln(n) + 172.1$	0.88	20 sandstone samples
Benavente et al. (2021)	$UCS = 137.656 - 4.953 n$	0.84	24 carbonate samples
Akin (2010)	$UCS = 44 e^{-0.11n}$	0.96	40 carbonates specimens
This study	$UCS = -5.0075 n_{(sb)} + 112.9$	0.48	12 Sandstone specimens
This study	$UCS = -0.5087 n_{(sb)} + 104.16$	0.005	12 carbonates specimens

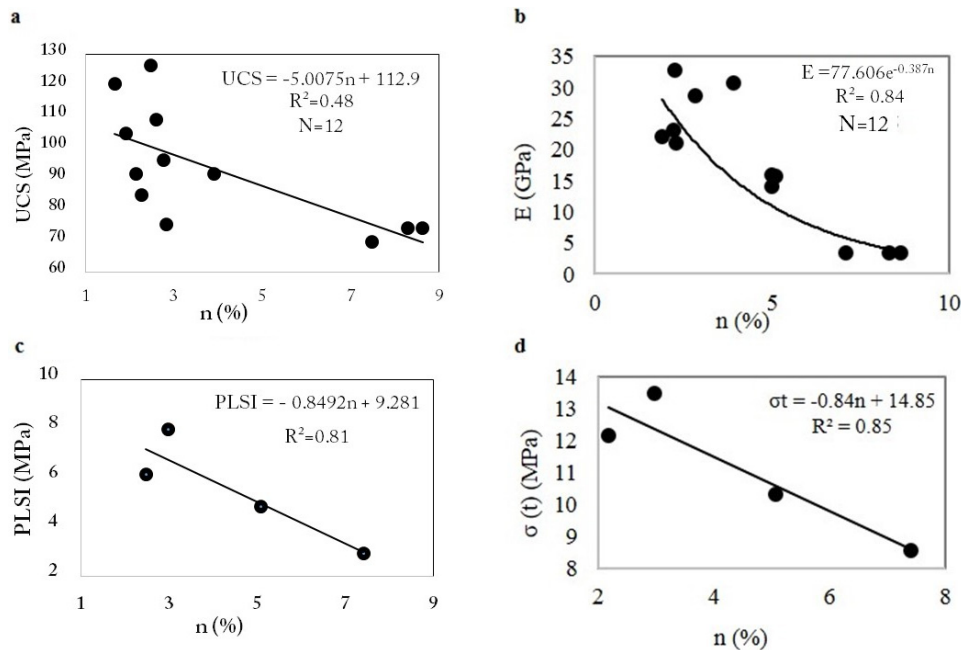


Figure 10. The relation between SB porosity and a) UCS, b) E, c) PLSI, d) σ_t in URS samples; In PLSI and σ_t graphs, each point is denoted as the mean value of three data resulted from tests

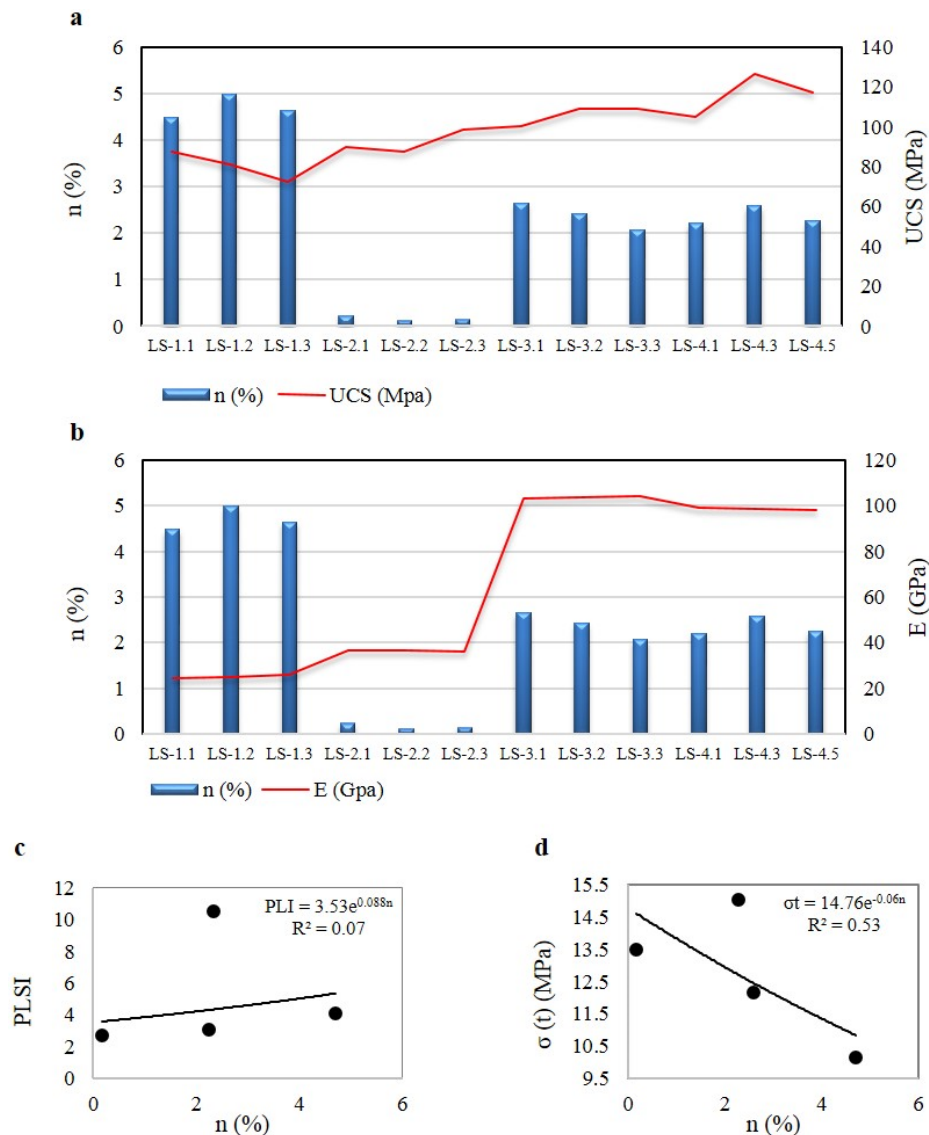


Figure 11. The relation between SB porosity and a) USC and b) E in AL samples (no important correlations are found); according to the graph, 3 core specimens from each block sample were used to assess the UCS and E; c) and d) the relations between SB porosity and PLSI and σ_t in AL samples, respectively. Each point is represented as the mean value of three data resulting from the tests

Hence, the relation between E and porosity resembles the UCS-porosity relation (Fig. 11a). As shown in Fig. 10c, according to some previous studies, a strong relation between porosity and PLSI ($R^2=0.81$) is observed in URS samples. In AL samples, no important correlation is found between porosity and PLSI (Fig. 11c). On the other hand, increased porosity can well reduce σ_t in both types of samples (Figs. 10d and 11d).

The relation between PIA porosity and other physical and mechanical properties

After calculating the porosity by the PIA method, the relation between PIA porosity and other rock features was studied as a beneficial approach to evaluate PIA’s advantages and disadvantages. Since porosity values obtained using the PIA in the AL samples were not remarkable, the investigation focused just on URS samples. As shown in Fig. 12a, a relatively weak correlation was found between PIA porosity and water absorption. This result suggests

that water absorption in URS is associated with the small-scale pores, which are not distinguishable from those of the PIA method. Figs. 12b and 12c display the relations between PIA porosity with PWVD and PWVS. According to the given graphs, there is a weak relation between PIA porosity and PWVD, with a correlation regression of about 44 (%). This weak relation reveals that the voids found by PIA are not the only agent to control the PWVD as other factors, such as cementation and planes of weakness, may control it. The decreasing trend of PWV in the sample of SS-2 is due to these distinguishable planes of weakness, leading to the deterioration of rock rigidity. The relation in saturated condition shows a poor correlation, too (Fig. 12c).

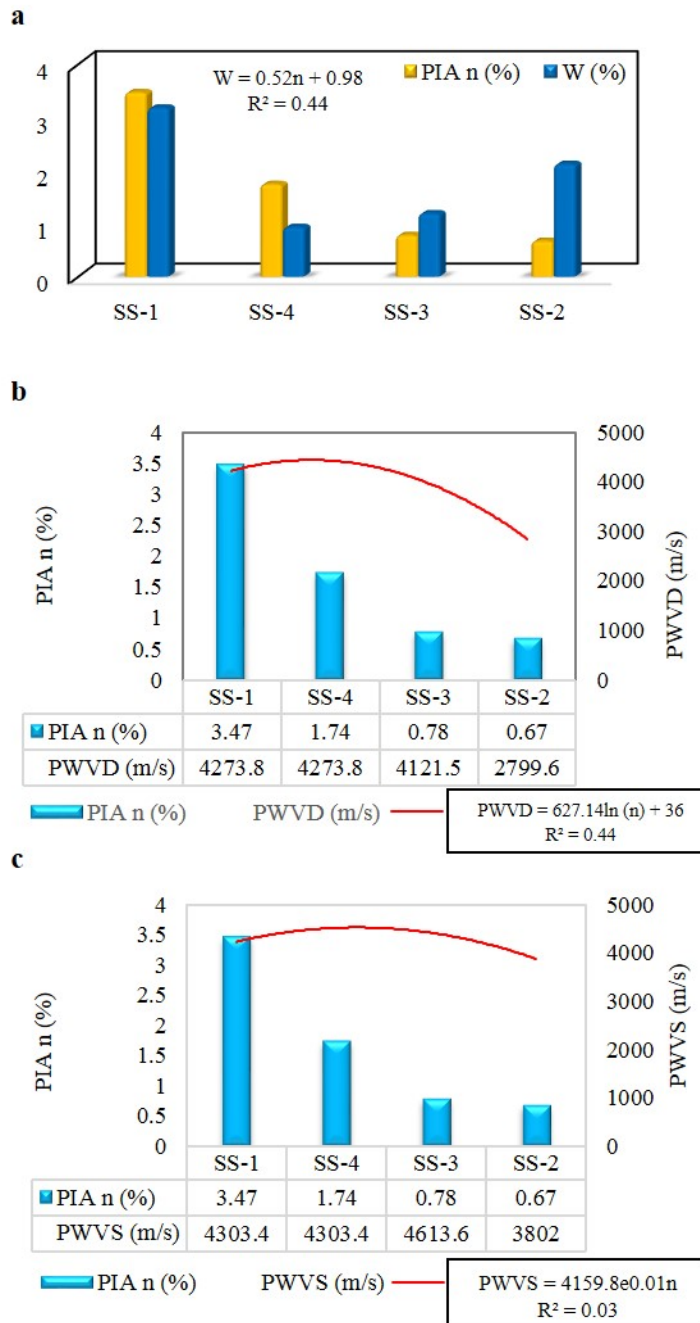


Figure 12. The relation between PIA porosity and a) water absorption, b) PWVD, and c) PWVS in the URS samples

Furthermore, there was a significant relation between PIA porosity and UCS ($R^2= 0.7$). Fig. 13c illustrates that as PIA porosity increases, the UCS decreases. In other words, pores identified via the PIA method cause URS samples to lose their rigidity and make them rather weak against external stresses. The obtained relation determines that meso- and macro-voids could control the UCS in URS. Also, a significant inverse relationship between PIA porosity and E was found (Fig. 13d) due to these meso- and macro-pores.

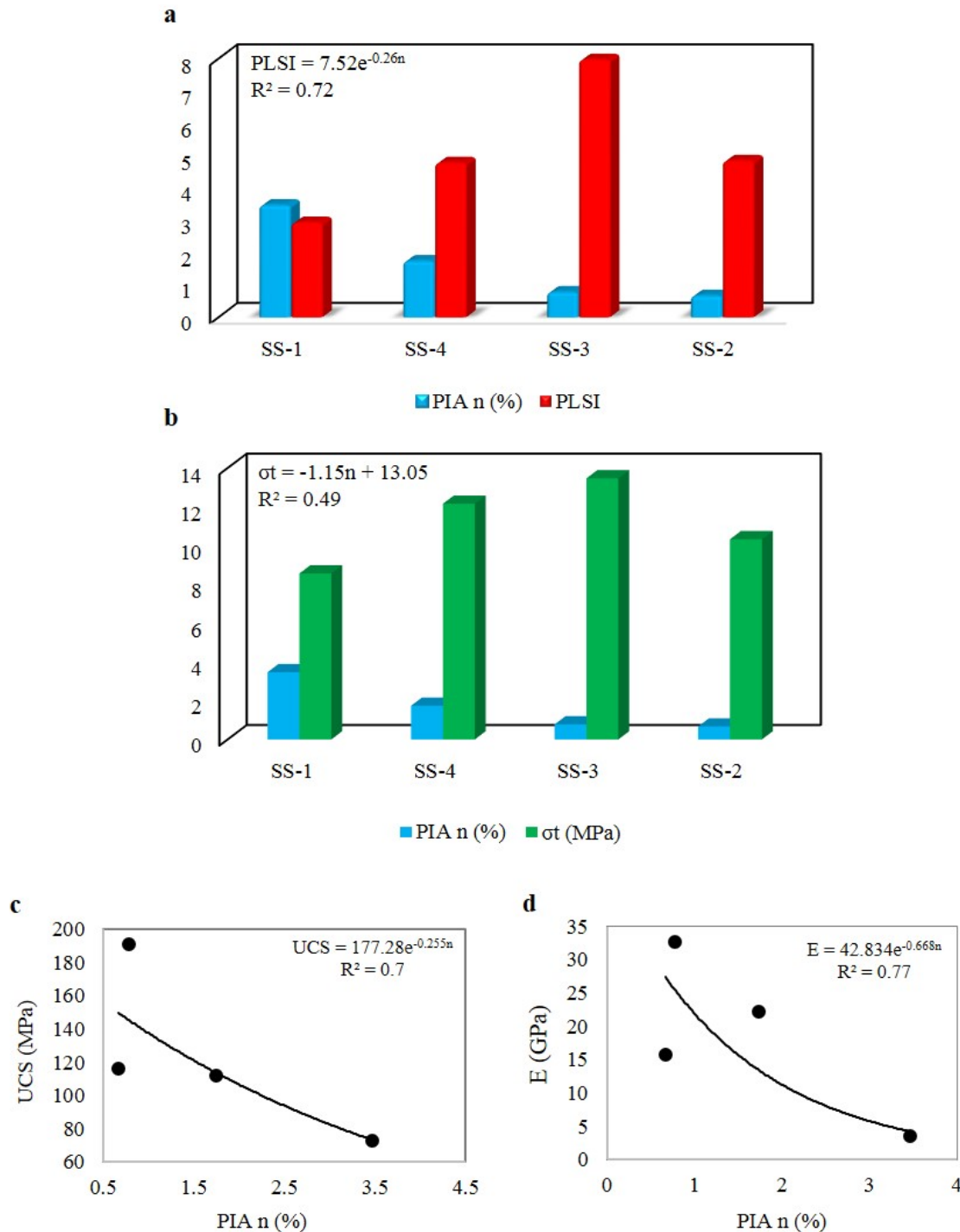


Figure 13. The relation between PIA porosity and a) UCS, b) E, c) PLSI, and d) σ_t in the URS samples

As given in Fig. 13a, a good relationship was established between PIA porosity and PLSI ($R^2= 0.72$). Decreasing PIA porosity increases PLSI. Also, sample SS-2 has the lowest PIA porosity among all samples, while it shows a moderate PLSI value compared to the other samples. This phenomenon is due to the plane of weakness of sample SS-2 resulting in a decrease in PLSI. In ideal conditions, by increasing the effective surfaces between mineral grains, the rock sample shows larger compressive and tensional strengths. Accordingly, a moderate relationship between PIA porosity and σ_t was found ($R^2= 0.49$), indicating that pores identified via PIA could not completely control the σ_t (Fig. 13b).

Conclusions

In this study, porosities of Upper Red Sandstones (URS) and Asmari Limestones (AL) were studied via Petrography Image Analysis (PIA) and Saturation-buoyancy (SB) methods. The major conclusions of this study are summarized as follows:

Comparing the PIA and SB results reveals that the PIA method underestimates the porosity both in URS and AL samples. This phenomenon can have two main reasons: 1) the failure of blue-dyed epoxy resin to fill the pores completely (i.e., micro, meso, and macro pores) and 2) incomplete imaging of petrographic microscope due to the limitation in microscope magnification.

The relationship between SB porosity and URS samples' physical and mechanical characteristics was investigated. The results exhibited a noticeable correlation between SB porosities and water absorption, E , and σ_t . a moderate correlation was established between SB porosity and PWVD, PWVS, UCS, and PLSI values.

In AL samples, PWVD, PWVS, σ_t , and water absorption showed good relation with SB porosity. In addition, it was determined that UCS and E had varied behavior versus SB porosity. Furthermore, no significant relation was extracted between SB porosity and PLSI in AL samples.

Acknowledgment

Financial support for this work by Tarbiat Modares University and Iran National Science Foundation (ISNF) (under grant number 99017809) is gratefully acknowledged. The authors are thankful to Mr. Milad Ghorbani and Yasin Kargar for their cooperation.

References

- Akin, M., 2010. A quantitative weathering classification system for yellow travertines. *Environ Earth Sci* 61(1): 47-61.
- Ahmadhadi, F., Daniel, J.M., Azzizadeh, M., Lacombe, O. (2008) Evidence for pre-folding vein development in the Oligo-Miocene Asmari Formation in the Central Zagros Fold Belt, Iran. *Tectonics* 27 (1).
- Alves, H., Lima, I., Assis, J.T., Geraldés, M., Lopes, R.T., 2014. Comparison of pore space features by thin sections and X-ray microtomography. *Appl Radiat Isot* 94:182-190.
- Andriani, G., Walsh, N., 2002. Physical properties and textural parameters of calcarenitic rocks: qualitative and quantitative evaluations. *Eng Geol* 67: 5-15.
- Anselmetti, F.S., Luthi, S., Eberli, G.P., 1998. Quantitative characterization of carbonate pore systems by digital image analysis. *AAPG Bull* 82:1815–1836
- Assefa, S., McCann, C., Sothcott, J., 2003. Velocities of compressional and shear waves in limestones. *Geophys Prospect* 51:1-13.
- Bell, F.G., Lindsay, P., 1999. The petrographic and geomechanical properties of some sandstones from the Newspaper Member of the Natal Group near Durban, South Africa. *Eng Geol* 53(1): 57-81.
- Benavente, D., García del Cura, M.A., Fort, R., Ordóñez, S., 2004. Durability estimation of porous

- building stones from pore structure and strength. *Eng Geol* 74:113-127.
- Benavente, D., Fort, R., Gomez-Heras, M., 2021. Improving uniaxial compressive strength estimation of carbonate sedimentary rocks by combining minimally invasive and non-destructive techniques. *Int. J. Rock Mech. Min. Sci* 147: 104915.
- Berrezueta, E. González-Menéndez, L. Ordóñez-Casado, B. Olaya, P., 2015. Pore network quantification of sandstones under experimental CO₂ injection using image analysis. *Comput Geosci* 77: 97-110.
- Boving, T.B and Grathwohl, P., 2001. Tracer diffusion coefficients in sedimentary rocks: correlation to porosity and hydraulic conductivity. *J Contam Hydrol* 53:85-100. [https://doi.org/10.1016/S0169-7722\(01\)00138-3](https://doi.org/10.1016/S0169-7722(01)00138-3)
- Cerepi, A. Humbert, L. Burlot, R., 2001. Petrophysical properties of porous medium from petrographic image analysis data. *Colloids Surf A Physicochem Eng Asp* 187: 233-256. [https://doi.org/10.1016/S0927-7757\(01\)00636-7](https://doi.org/10.1016/S0927-7757(01)00636-7)
- Chang, C., Zoback, M. D., Khaksar, A., 2006. Empirical relations between rock strength and physical properties in sedimentary rocks. *J Pet Sci Eng* 51(3-4): 223–237.
- Choquette, P.W and Pray, L.C., 1970. Geologic nomenclature and classification of porosity in sedimentary carbonates. *AAPG bulletin* 54(2): 207-250.
- Dehghanian, M.S. Khosrotehrani, K. Afghah, M. Keshani, F (2012) Microfacies study of Asmari formation in the northwest and southeast of Shiraz, Iran. *Advances in Environmental Biology* 6(2): 556-563.
- Di Benedetto, C. Cappelletti, P. Favaro, M. Graziano, S.F. Langella, A. Calcaterra, D. Colella, A., 2015. Porosity as key factor in the durability of two historical building stones: Neapolitan Yellow Tuff and Vicenza Stone. *Eng Geol* 193:310-319.
- Dunham, R.J (1962) Classification of carbonate rocks according to depositional texture. In: Ham, W.E. (Ed.), Classification of carbonate rocks. *Am. Assoc. Pet. Geol. Mem.*, 1: 108–12.
- Erdoğan, O., Özvan, A (2015) Evaluation of strength parameters and quality assessment of different lithotype levels of Edremit (van) travertine (eastern Turkey). *Afr Earth Sci* 106:108-117.
- Farrell, N.J.C. Healy, D. Taylor, C.W (2014) Anisotropy of permeability in faulted porous sandstones. *J Struct Geol* 63:50-67.
- Farrokhrouz, M., Asef, M. R., 2017. Experimental investigation for predicting compressive strength of sandstone. *J Nat Gas Sci Eng* 43: 222-229.
- Folk, R.L (1962) Spectral subdivision of limestone types. In: Ham, W.E. (Ed.), Classification of Carbonate Rocks. *Am. Assoc. Pet. Geol. Mem.*, 1: 62-84, Tulsa.
- Folk, R.L (1974). Petrology of sedimentary rocks. Austin, Texas, Hemphill, 182.
- Freire-Lista, D. M., Fort, R., Varas-Muriel, M. J. 2015. Freeze–thaw fracturing in building granites. *Cold Reg. Sci. Technol.*, 113, 40-51.
- Freire-Lista, D.M., Fort, R. and Varas-Muriel, M.J., 2016. San Pedro leucogranite from A Coruña, Northwest of Spain: Uses of a heritage stone. *Energy Procedia.*, 97: 554-561. <https://doi.org/10.1016/j.egypro.2016.10.075>
- Freire-Lista, D. M., Gonçalves, G. V., Vazquez, P., 2022. Weathering detection of granite from three asynchronous historical quarries of Sabrosa municipally (North Portugal). *J. Cult. Herit*, 58: 199-208. <https://doi.org/10.1016/j.culher.2022.10.008>
- Galaup, S. Liu, Y. Cerepi, A., 2012. New integrated 2D–3D physical method to evaluate the porosity and microstructure of carbonate and dolomite porous system. *Microporous Mesoporous Mater.* 154, 175-186.
- Ghasemi, S. Khomehchiyan, M., Taheri, A., Nikudel, M.R., Zalooli, A., 2021. Microcracking behavior of gabbro during monotonic and cyclic loading. *Rock Mech Rock Eng* 54: 2441-2463.
- Ghiasi-Freer, J. Soleimanpour, I. Kadkhodaie-Ilkhchi, A. Ziaii, M. Sedighi, M. Hatampour, A., 2012. Semi-automated porosity identification from thin section images using image analysis and intelligent discriminant classifiers. *Comput Geosci* 45:36-45.
- Ghobadi, M.H and Babazadeh, R., 2015a. An investigation on the effect of accelerated weathering on strength and durability of Tertiary sandstones (Qazvin province, Iran). *Environ Earth Sci* 73(8):4237-4250.
- Ghobadi, M.H., Babazadeh, R., 2015b. Experimental studies on the effects of cyclic freezing–thawing, salt crystallization, and thermal shock on the physical and mechanical characteristics of selected

- sandstones. *Rock Mech Rock Eng* 48:1001-1016.
- Ghobadi, M., Babazadeh, R., 2016. The assessment of salt weathering and freeze-thaw effect on strength and durability of upper red formation sandstones. *jeg.* 10 (1):3351-3378.
- Grove, C and Jerram, D.A., 2011. jPOR: An ImageJ macro to quantify total optical porosity from blue-stained thin sections. *Comput Geosci* 37:1850-1859.
- Haines, T.J., Neilson, J.E., Healy, D., Michie, E.A., Aplin, A.C., 2015. The impact of carbonate texture on the quantification of total porosity by image analysis. *Comput Geosci* 85:112-125. <https://doi.org/10.1016/j.cageo.2015.08.016>
- Higgins, M.D. 2006. Quantitative textural measurements in igneous and metamorphic petrology. Cambridge University Press, Cambridge. <https://doi.org/10.1017/CBO9780511535574>
- ISRM 2007. Rock characterization, testing and monitoring. In: Brown ET (ed) International society of rock mechanics suggested methods. Pergamon Press, Oxford 1-211.
- James, R.A., 1995. Application of petrographic image analysis to the characterization of fluid-flow pathways in a highly-cemented reservoir: Kane Field, Pennsylvania, USA. *J Pet Sci Eng* 13:141-154.
- Jamshidi A, Nikudel MR, Khamechiyan M., 2013. Estimating the durability of building stones against Salt crystallization: considering the physical properties and strength characteristics. *Geopesia* 3:35-48.
- Jamshidi A., Nikudel M.R., Khamehchiyan, M., Zalooli, A., 2015. Statistical models for predicting the mechanical properties of travertine building stones after freeze-thaw cycles. In: Lollino G et al. (eds) *Engineering geology for society and territory*, Springer, Heidelberg, 8: 477-481.
- Jamshidi A, Nikudel MR, Khamehchiyan M., 2016. Evaluation of the durability of Gerdoee travertine after freeze–thaw cycles in fresh water and sodium sulfate solution by decay function models. *Eng Geol* 202:36-43.
- Jamshidi A, Nikudel MR, Khamehchiyan M, Zalooli A, Yeganehfar H., 2017. Estimating the mechanical properties of travertine building stones due to salt crystallization using multivariate regression analysis. *J Sci I R Iran* 28: 231–241.
- Jamshidi, A., Zamanian, H., Zarei Sahamieh, R., 2018. The effect of density and porosity on the correlation between uniaxial compressive strength and P-wave velocity. *Rock Mech Rock Eng*, 51, 1279-1286.
- Jamshidi, A., 2022. A Comparative Study of Point Load Index Test Procedures in Predicting the Uniaxial Compressive Strength of Sandstones. *Rock Mech Rock Eng* 55: 4507-4516.
- Jeng, F.S. Weng, M.C. Lin, M.L. Huang, T.H., 2004. Influence of petrographic parameters on geotechnical properties of tertiary sandstones from Taiwan. *Eng Geol* 73:71-91.
- Kahraman, S. Gunaydin, O. Fener, M., 2005 The effect of porosity on the relation between uniaxial compressive strength and point load index. *Int J Rock Mech Min Sci* 42: 584-589. <https://doi.org/10.1016/j.ijrmms.2005.02.004>
- Kassab, M. A., Weller, A., 2015. Study on P-wave and S-wave velocity in dry and wet sandstones of Tushka region, Egypt. *Egypt J Pet* 24(1): 1-11.
- Khanlari, G and Abdilor, Y., 2015. Influence of wet-dry, freeze-thaw, and heat-cool cycles on the physical and mechanical properties of upper red sandstones in central Iran. *Bull Eng Geol Environ* 74:1287–1300.
- Khanlari, G. Sahamieh, R.Z. Abdilor, Y., 2014. The effect of freeze–thaw cycles on physical and mechanical properties of Upper Red Formation sandstones, central part of Iran. *Arab J Geosci.* <https://doi.org/10.1007/s12517-014-1653-y>
- Khosrow Tehrani, K., 1989. Stratigraphy of Iran and type sections of the formations. Tehran. Tehran University pp. 353
- Lasemy, Y., 1990. Depositional environments of Upper Red formation. 9th earth science symposium. Tehran. Geological Survey of Iran.
- Martínez-Martínez, J. Benavente, D. García Del Cura, M.A., 2007. Petrographic quantification of brecciated rocks by image analysis. Application to the interpretation of elastic wave velocities. *Eng Geol* 90:41-54.
- Mishra, D.A and Basu, A., 2013. Estimation of uniaxial compressive strength of rock materials by index tests using regression analysis and fuzzy inference system. *Eng Geol* 160:54-68. <https://doi.org/10.1016/j.enggeo.2013.04.004>
- Moradi, M. Moussavi-Harami, R. Mahboubi, A. Khanehbad, M. Ghabeishavi, A (2017) Rock typing

- using geological and petrophysical data in the Asmari reservoir, Aghajari Oilfield, SW Iran. *J Pet Sci Eng* 152:523-537.
- Motiei, H., 1993. Stratigraphy of Zagros. Geological survey of Iran, pp 583
- Nabawy, B.S., 2014. Estimating porosity and permeability using digital image analysis (DIA) technique for highly porous sandstones. *Arab J Geosci* 7(3):889-898.
- Najibi, A.R. Ghafoori, M. Lashkaripour, G.R., 2015. Empirical relations between strength and static and dynamic elastic properties of Asmari and Sarvak limestones, two main oil reservoirs in Iran. *J Pet Sci Eng* 126:78-82.
- Neto, I.A.L. Misságia, R.M. Ceia, M.A. Archilha, N.L. Oliveira, L.C., 2014. Carbonate pore system evaluation using the velocity–porosity–pressure relationship, digital image analysis, and differential effective medium theory. *J Appl Geophys* 110:23-33.
- Obara, B., 2007. Identification of transcrySTALLINE microcracks observed in microscope images of a dolomite structure using image analysis methods based on linear structuring element processing. *Comput Geosci* 33(2):151-158.
- Pappalardo, G. Punturo, R. Mineo, S. Contrafatto, L., 2017. The role of porosity on the engineering geological properties of 1669 lavas from Mount Etna. *Eng Geol* 221:16-28.
- Paxton, S.T. Szabo, J.O. Ajdukiewicz, J.M. Klimentidis, R.E., 2002. Construction of an intergranular volume compaction curve for evaluating and predicting compaction and porosity loss in rigid-grain sandstone reservoirs. *AAPG Bull* 86: 2047–2067.
- Peng, S. Hassan, A. Loucks, R.G., 2016. Permeability estimation based on thin-section image analysis and 2D flow modeling in grain-dominated carbonates. *Mar Petrol Geol* 77:763-775.
- Perring, C.S. Barnes, S.J. Verrall, M.H.R., 2004. Using automated digital image analysis to provide quantitative petrographic data on olivine-phyric basalts. *Comput Geosci* 30:183-195. <https://doi.org/10.1016/j.cageo.2003.10.005>
- Pettijohn, F.J., 1975. *Sedimentary rocks* (Vol. 3). New York. Harper & Row.
- Přikryl, R., 2006. Assessment of rock geomechanical quality by quantitative rock fabric coefficients: Limitations and possible source of misinterpretations. *Eng Geol* 87:149-162. <https://doi.org/10.1016/j.enggeo.2006.05.011>
- Qi, Y., Ju, Y., Yu, K., Meng, S., Qiao, P., 2022. The effect of grain size, porosity and mineralogy on the compressive strength of tight sandstones: A case study from the eastern Ordos Basin, China. *J Pet Sci Eng* 208: 109461. <https://doi.org/10.1016/j.petrol.2021.109461>
- Rabbani, A., Assadi, A., Kharrat, R., Dashti, N., Ayatollahi, S., 2017. Estimation of carbonates permeability using pore network parameters extracted from thin section images and comparison with experimental data. *J. Nat. Gas Sci. Eng.*, 42, pp. 85–98. <https://doi.org/10.1016/j.jngse.2017.02.045>
- Ruzyla, K., 1986. Characterization of pore space by quantitative image analysis. *SPE Form Eval* 1(04):389-398.
- Scholle, P.A and Ulmer-Scholle, D.S., 2003. A color guide to the petrography of carbonate rocks: grains, textures, porosity, diagenesis. *AAPG Mem* 77:1–474.
- Shaeri, J. Mahdavinjad, M., Zalooli, A., 2022. Physico-mechanical and Chemical Properties of Coquina Stone Used as Heritage Building Stone in Bushehr, Iran. *Geoheritage*. 14(3): 95. <https://doi.org/10.1007/s12371-022-00738-0>
- Solymar, M and Fabricius, I.L (1999) Image analysis and estimation of porosity and permeability of Arnager greensand, Upper Cretaceous, Denmark. *Phys Chem Earth Solid Earth Geodes* 24(7): 587-591.
- Sousa, L.M.O. Suarez del Rio, L.M. Calleja, L. Ruiz de Argondona, V.G. Rey, A.R., 2005. Influence of microfractures and porosity on the physico-mechanical properties and weathering of ornamental granites. *Eng Geol* 77: 153-168.
- Stueck, H., Koch, R., Siegesmund, S., 2013. Petrographical and petrophysical properties of sandstones: statistical analysis as an approach to predict material behaviour and construction suitability. *Environ Earth Sci* 69: 1299-1332.
- Török, Á., Vársárhelyi, B., 2010. The influence of fabric and water content on selected rock mechanical parameters of travertine, examples from Hungary. *Eng Geol*, 115(3-4): 237-245.
- Tucker, M.E., 2009. *Sedimentary petrology: an introduction to the origin of sedimentary rocks*. John Wiley & Sons.
- Tuğrul, A., 2004. The effect of weathering on pore geometry and compressive strength of selected rock

- types from Turkey. *Eng Geol* 75:215-227.
- Tugrul, A and Zarif, I.H., 1999. Correlation of mineralogical and textural characteristics with engineering properties of selected granitic rocks from Turkey. *Engng. Geol.* 51:303-317.
- Wennberg, O. Svåná, T. Azizzadeh, M. Aqravi, A. Brockbank, P. Lyslo, K. Ogilvie, S., 2006 Fracture intensity vs. mechanical stratigraphy in platform top carbonates: the Aquitanian of the Asmari Formation, Khaviz Anticline, Zagros, SW Iran. *Pet Geosci* 12: 235-246.
- Zalooli, A., Khamsehchiyan, M., Nikudel, M.R. and Jamshidi, A., 2017. Deterioration of travertine samples due to magnesium sulfate crystallization pressure: examples from Iran. *Geotech Geol Eng.*35: 463-473.
- Zalooli, A. Freire-Lista, D.M. Khamsehchiyan, M. Nikudel, M.R. Fort, R. Ghasemi, S (2018a) Ghaleh-khargushi rhyodacite and Goid andesite from Iran: characterization, uses, and durability. *Environ Earth Sci* 77: 315. <https://doi.org/10.1007/s12665-018-7485-4>
- Zalooli, A. Khamsehchiyan, M. Nikudel, M.R., 2018b. The quantification of total and effective porosities in travertines using PIA and saturation-buoyancy methods and the implication for strength and durability. *Bull Eng Geol Environ.* 77(4): 1739-1751.
- Zalooli, A. Khamsehchiyan, M. Nikudel, M.R. Freire-Lista, D.M. Fort, R. and Ghasemi, S., 2020. Artificial microcracking of granites subjected to salt crystallization aging test. *Bull Eng Geol Environ.* 79: 5499-5515.
- Zorlu, K. Gokceoglu, C. Ocakoglu, F. Nefelioglu, H.A. Acikalin, S., 2008. Prediction of uniaxial compression strength of sandstones using petrography-based models. *Eng Geol* 96(3/4):141-158.



This article is an open-access article distributed under the terms and conditions of the Creative Commons Attribution (CC-BY) license.